universe

IMPACT FACTOR 2.5

CITESCORE 4.3

Article

Probing the Nonlinear Density Wave Theory of Spiral Galaxies by Baryonic Tully–Fisher Relation

Miroslava Vukcevic, Djordje Savic and Predrag Jovanović

Special Issue

Recent Advances in Gravitational Lensing and Galactic Dynamics

Edited by

Dr. Francesco De Paolis, Prof. Dr. Alexander F. Zakharov and Prof. Dr. Luka Č. Popović

MDPI

https://doi.org/10.3390/universe10090359

universe

MDPI

Article

Probing the Nonlinear Density Wave Theory of Spiral Galaxies by Baryonic Tully–Fisher Relation

Miroslava Vukcevic *, Djordje Savic and Predrag Jovanović

Astronomical Observatory Belgrade, Volgina 7, 11000 Belgrade, Serbia; djsavic@aob.rs (D.S.); pjovanovic@aob.rs (P.J.)

* Correspondence: vuk.mira@gmail.com

Abstract: The baryonic mass–velocity relation provides an important test of different galaxy dynamics models such as Lambda–cold dark matter (ΛCDM) and alternatives like Modified Newtonian Dynamics (MOND). Novel nonlinear density wave theory with a soliton solution gives an opportunity to test whether the derived rotational velocity expression is able to support the well known Tully–Fisher empirical relation between mass and rotation velocity in disk galaxies. Initial assumptions do not involve any larger dark matter halo that supports the stability of the very thin galactic disk nor any modified gravitational acceleration acting on galactic scales. It rather follows an important gravitational interaction between constituents of disk mass in the outer part of the disk via gravitational potential. Data are obtained by a fitting procedure applied on the sample of 81 rotational curves of late type spirals using expressions for the rotational velocity derived as an exact, a self-consistent solution of the nonlinear Schrodinger (NLS) equation for galactic surface mass density. The location of these selected objects in the baryonic mass–rotation velocity plane follows the relation $\log \mathcal{M}_b = (3.7 \pm 0.2) \log V_{flat} + (2.7 \pm 0.4)$ in marginal agreement with the findings in the literature.

Keywords: gravity; galaxy dynamics; nonlinear waves

Citation: Vukcevic, M.; Savic, D.; Jovanović, P. Probing the Nonlinear Density Wave Theory of Spiral Galaxies by Baryonic Tully–Fisher Relation. *Universe* **2024**, *10*, 359. https://doi.org/10.3390/universe10090359

Academic Editor: Stephen J. Curran

Received: 22 July 2024
Revised: 27 August 2024
Accepted: 3 September 2024
Published: 6 September 2024

1. Introduction

The Tully–Fisher relation [1] was originally derived as an empirical relation between optical luminosity and the width of the 21 cm line, so that it is one of the strongest empirical correlations in extragalactic astronomy. Apart from its use as a distance indicator [2], it is used as a constraint on galaxy-formation models [3–5], as well as a test of theories that seek to modify gravity in order to obviate the need for dark matter [6–8]. It has been pointed out that baryonic mass is a more fundamental quantity than luminosity [9–11]. Even more, it has been shown that not only mass, but also the specific distribution of the mass, plays an essential role in galactic dynamics, and consequently, in the shape of rotation velocity curves [12]. Both types of baryonic mass, gaseous and stellar component, contribute to a baryonic Tully–Fisher relation (BTFR): $\mathcal{M}_b = AV^\alpha$, which is linear with respect to mass (in log space) [10,11,13–19], so that BTFR is the general physical relation supporting the empirical Tully–Fisher relation.

In this paper, we provide an independent calibration of the BTFR with galactic mass derived using the nonlinear spiral soliton solution applied on the observed RCs (rotational curves) for a sample of late-type spirals found in the Spitzer Photometry and Accurate Rotation Curves (SPARC) database Lelli et al. [20] as a compiled representative sample of different types of spiral non-bared galaxies. The disk masses of spiral galaxies are estimated for stellar components but the gaseous contribution can be added since gas follows similar spiral configurations [21].

Our results are compared with the canonical relation provided by Lelli et al. [19]. The nonlinear approach was used by Henriksen [22] but using a kinetic model combined with an orbital method, which is a different type of nonlinearity to that considered in this work.

In Section 2, we recall the analytically, self-consistently derived expression for rotational velocity without assuming either gravity potential or mass distribution. Data selection and model setup are described in Section 3. The fitting procedure is explained in Appendix A. We elaborate our main results and BTFR in Sections 4 and 5. Individual fit results for each galaxy are listed in Appendix B. A summary and conclusions are given in Section 6.

2. Nonlinear Density Wave Solution and Consequent Rotational Velocity Expression

Circular velocity V at certain radius r of the rotating stellar galactic disk is defined by gravity potential ϕ as

$$V^2(r) = r\frac{\partial \phi}{\partial r}. \tag{1}$$

The main difficulty in the galactic dynamics is mutual influence of the mass distribution and gravity potential, accompanied by the rotation effects and geometry. If the system is treated by a standard set of non-collision hydrodynamic equations, it has to be fulfilled by Poisson's equation for the potential. The set of equations is nonlinear. The linearized model proposed by Lin and Shu [23], known as density wave theory, has been widely used more than six decades after [24]. Linear density waves are dispersive, meaning that different wave numbers move with different velocities, and would be blown away in a period shorter than it would be possible to observe them. Nonlinear density wave theory itself would not ensure the endurance of such waves, but the existence of solitons can ensure their endurance. So nonlinear effects play an essential role in competing in the dispersion effects, creating stable solutions under certain circumstances. In galactic dynamics, such a circumstance is the marginal stability of the disk, allowing the creation of solitons. Physically, a nonlinear soliton solution is extremely important in several aspects [25]:

1. It ensures a long-lasting spiral structure, longer than one rotation period due to transport of the mass at outer regions of the disk by the soliton wave; this is the reason why the disk remains at the threshold of instability for a long time, much longer than in linearized density wave theory, for more than a few Gy;
2. The existence of such a solution guaranties constant wave group velocity, as long as the condition for existence is satisfied (marginal stability of the disk; for details, see [25]), which means that all particles trapped by the wave exhibit the same velocity,
3. The existence of the soliton solution of the NLS equation provides a brief, fine structure within the envelope soliton, much shorter than the width of a soliton; this can explain the formation of large density gradients within the spiral arm responsible for star formation;
4. At the edge of the disk, the soliton would increase its width and velocity due to its amplitude, which can explain the disk mass density fall off with a radius faster than 1/r.

We proceed to approximating the gravity potential gradient in Equation (1) as:

$$\frac{\partial \phi}{\partial r} = r\Omega^2 + \sum_{\infty}^{n=1} \sum_{m=-\infty}^{\infty} 2\pi G \epsilon^n \Re(\rho^{(n,m)}(\xi,\eta) e^{i(kr-\omega\tau)}), \tag{2}$$

where Ω is the angular velocity defined as v/r, G is the gravitational constant, ξ and η are stretched spatial and temporal coordinates, ρ is the perturbation of the surface mass density (SMD), and k and ω are wave number and frequency, respectively. The sign $\Re$ indicates that only the real part of the variable has to be taken into account, τ is the time variable evaluated to the period of rotation and ϵ is the small parameter related with the marginal stability condition. Next, SMD is replaced by the exact solution of NLS [25] which

is a bright soliton (enhanced density along the spiral) presented in Figure 1, resulting in the expression for circular velocity as follows:

$$V(r) = \sqrt{\Omega^2 r^2 + \frac{ar}{\cosh b(T - cr)}}. \quad (3)$$

Parameters a, b, and c are defined as in previous works [12,25,26]:

$$a = 2\pi G\rho_0\rho_a(3 \times 10^{16})[\text{km s}^{-2}], \quad (4)$$

$$b = \kappa\rho_a(3 \times 10^{16})[\text{s}^{-1}], \quad (5)$$

$$c = \frac{\kappa}{2\pi G\rho_0} = \frac{1}{V_g}[\text{s km}^{-1}], \quad (6)$$

where κ is epicyclic frequency due to differential rotation, ρ_0 is unperturbed surface mass density, ρ_a is wave amplitude, and T is period of rotation. Epicyclic frequency κ is directly related to angular velocity Ω as a consequence of the conservation of angular momentum: inward (or outward) displacement of the star regarding its circular orbit results in the feedback force causing epyciclic motion, returning the star to the guiding orbit. V_g is the already mentioned group velocity of the density wave. An illustration of an exact solution of the NLS equation is shown in Figure 1 for a density-perturbation pattern in polar coordinates. We note that SMD and gravitational potential are phase shifted for $\pi/2$, which means that the maximum of the density takes place where the minimum of the potential is, ensuring that particles are trapped by the gravity potential along the spiral pattern. Since the dynamics is treated using wave phenomena, the same pattern follows the group velocity of the formed wave, which transports the energy of the wave. The present study includes azimuthally averaged SMD since the density perturbation (and all other variable perturbations, consequently) is φ-dependent in linear theory [23] as well as in nonlinear theory via $\tau = t - \varphi/\Omega$ stretched time coordinates. The dispersion relation contains Doppler-shifted frequency $\omega = (\omega - m\Omega)$, where m is the number of arms and

$$\varphi = (k(r) + C)/m, \quad (7)$$

while $k(r)$ is the wave number, φ is the polar or azimuth angle and C is an arbitrary constant. The spiral pattern is a curve on which the phase $exp(kr - \omega\tau)$ is constant.

Derivation of the rather general circular velocity expression (Equation (3)) is made with minimum assumptions, ones that approximate Poisson's equation to an infinitesimally thin disk. As to the gas component contribution in the total disk mass, it has been discussed in [12]. The addition of a gas component would slightly modify the rotational velocity but it will not modify drastically the overall shape of the rotation curve. Concerning this work, it will definitely make minor changes in the parameters a, b and c involving the velocity dispersion of the gaseous component but it will not significantly influence the conclusion, at least not more than a few percentages for regular spiral galaxies. Note that the relation $a = b/c$ reduces the number of free variables in the fitting procedure. The derivation of the NLS equation for the gaseous disk has been carried out in [21]; the spiral pattern exists but it will not coincide with the stellar one, as observations suggest. Analysis of the gaseous disk suggests importance in gas-rich dwarf galaxy dynamics as well as in the dynamics of accretion disks.

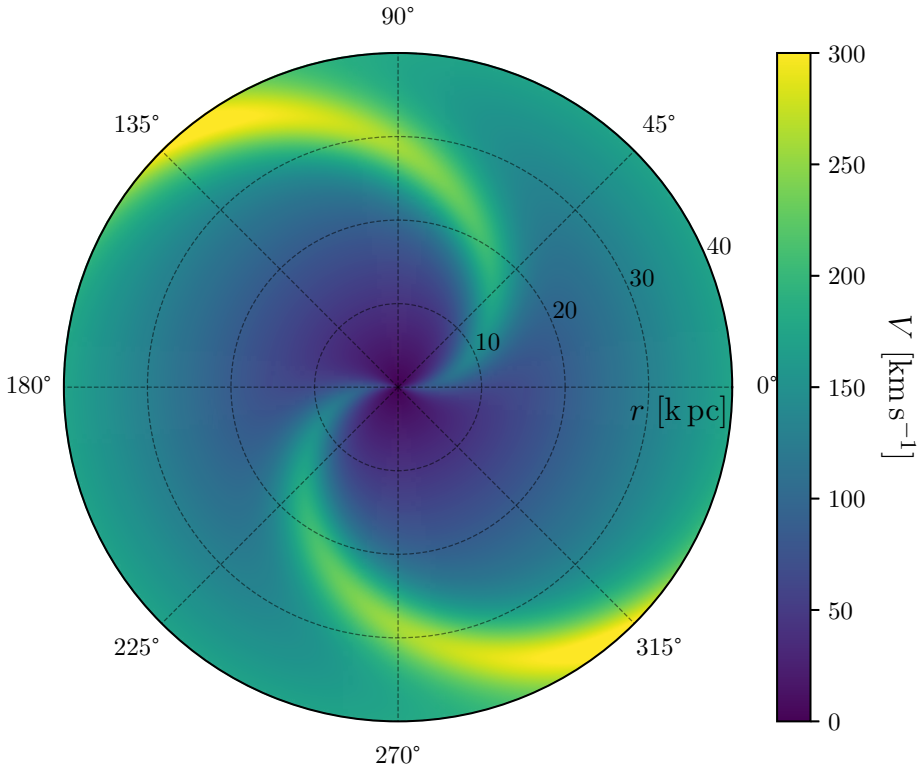

Figure 1. An example of a spiral pattern as a solution of the NLS equation (for details, see [12,21,25,26]). The colorbar indicates density magnitude.

3. Methods

The general form of the Equation (3) assumes that κ and ρ_0 depend on radius (e.g., power-law surface mass profile) as long as the ratio $\kappa(r)/\rho_0(r) = const$ holds. Fitting Equation (3) to the observed rotational velocity allows us to directly infer parameters a, b and c which are connected with the differential rotation κ, SMD ρ_0, wave amplitude ρ_a and the soliton group velocity V_g computing time parameter T and the total baryonic mass $\mathcal{M}_b$. The total stellar disk mass is integrated as $\mathcal{M}_b = 2\pi\rho_0 R^2$, where R corresponds to the maximum distance measured.

Here, it is necessary to discuss mass estimation: it has been underlined in the Introduction that not only mass, but also mass distribution, play an essential role in RC construction. The theoretical model of the RC needs to treat mutual gravitational interactions between stars in the outer part of the disk the influence of which is stronger than the influence of the gravity of the black hole placed in the bulge, since the disk mass contains 2/3 of the total galactic mass while on a bulge, together with a black hole, there is 1/3 of the total mass. This mutual interaction is governed by the spiral gravity potential formed along the disk. In the RC recovery, it was necessary to estimate parameters a, b and c using observed data for SMD and angular velocity or κ. In this research, estimation of the galactic disk mass via a fitting procedure using a theoretically derived rotation velocity expression (Equation (3)) is the subject of derived parameters a, b and c. As was already discussed, parameter c must be constant due to the existence of a soliton solution, representing the wave group velocity even though it is the ratio of two radial functions SMD and κ. In the opposite task, even though a and b are supposed to be radially dependent (see Equations (4) and (5)) we adopt constant, evaluated values by fitting. Consequently, SMD is taken as a constant instead of an exponential function with respect to the radius. Checking the M31 galaxy parameters from the sample used in the fitting procedure, overestimation of the disk mass was about 0.3 due to the constant SMD compared to the averaged pure exponential distribution; the exact percent depends strongly on the total radius, scale radius and SMD at a certain radius.

The strong impact on the estimated value of the disk mass has terminal velocity as well; that will be discussed in Section 5.

We kept estimated mass as simple as possible, with constant surface mass distribution with no loss of generality. However, we are aware that distribution of the mass is of crucial importance in the shape of the velocity curve [12], but in the opposite procedure, estimation of the mass using the velocity curve, it plays a role only as a multiplication factor of 1.3 at most. This is discussed in Section 5. Parameters r, κ, ρ_0 and T are expressed in kpc, $kms^{-1}kpc^{-1}$, $M_\odot pc^{-2}$ and $year$, respectively. Wave amplitude ρ_a is dimensionless. Details of the optimization procedure for fitting Equation (3) to models are given in Appendix A.

We use the kinematic RC measurements obtained for late-type spiral and irregular galaxies found in the SPARC (http://astroweb.cwru.edu/SPARC/, accessed on 20 July 2024) database [19,20]. For the M31 (Andromeda) galaxy, we use the data from Corbelli et al. [27]. The quality of data measurements varies from object to object, both in the number of measurements as well as errors. The errors in observed velocity represent both standard error and uncertainty in the circular velocity due to asymmetry in the velocity field [28]. We removed from the sample those objects with less than 10 data points in order to ensure a good quality of the fit, leaving us with a subset of 115 galaxies covering a wide range of galaxy types, sizes and velocity profiles. We perform no binning nor any re-sampling technique.

4. Results

The quality of the fit was inspected for each galaxy by careful analysis of the fit parameters and associated errors and by visually inspecting each graph.

We keep the same fit quality notation as Lelli et al. [20]: 1 (`High`), 2 (`Medium`), 3 (`Low`). The results of the fit are shown in Figure 2 (upper right panel) for several galaxies of various sizes and RC profiles. Individual plots for each galaxy are listed in the Appendix B. We find that the formula is capable of reproducing the observed rotational curves for 81 objects with high and medium quality. The mass we obtained for M31 $\mathcal{M}_b = 3.26 \pm 0.17e11[M_\odot]$ is in agreement with the mass estimated using kinematical data of planetary nebulae [29], globular clusters [30] and HI dynamics [31,32].

For the reduced sample of 81 galaxies, the distribution of model parameters as well as $\mathcal{M}_b$ and V_g is given in Figure 2 (left panels).

Regarding the fit parameters and their errors, we note that Equation (3) is the most sensitive to T, for which the relative error is often close to or larger than 1, while the other parameters remain stable, most notably κ and ρ_0. We point out a remarkably tight correlation between V_g and $\mathcal{M}_b$ (Figure 2, bottom second to the right panel).

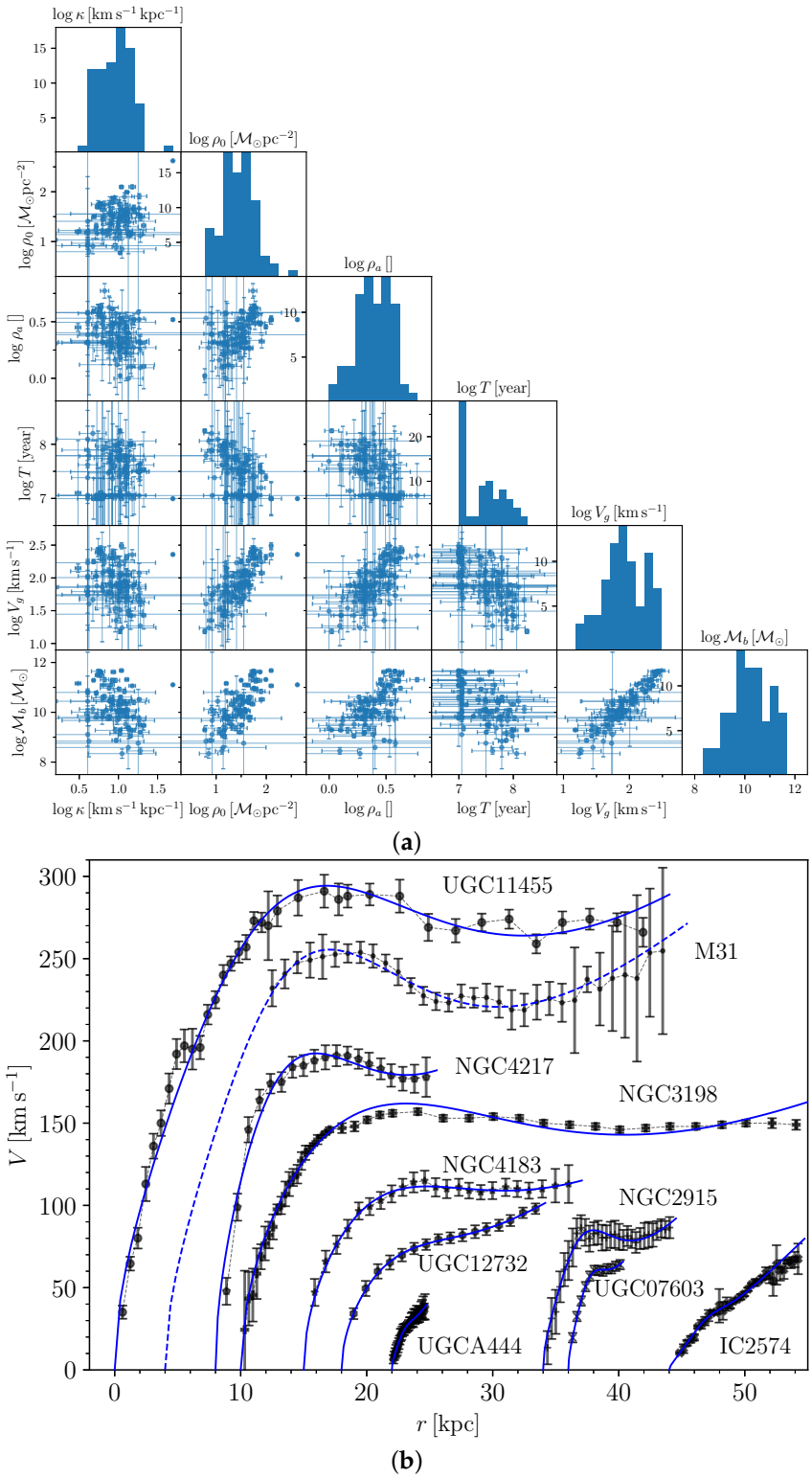

Figure 2. (**a**) Correlations of the fit parameters and computed Vg and galaxy mass for the 81 galaxies with high and medium fit quality. For clarity, we used log − log convention. Cumulative distributions are shown on the main diagonal for κ $[kms^{-1}kpc^{-1}]$, ρ_0 $[M_\odot pc^{-2}]$, ρ_a, T [year], V_g [km s^{-1}] and $\mathcal{M}_b$ $[M_\odot]$. (**b**) Observed rotation curves for M31 and UGC11455, NGC4217, NGC3918, NGC4183, UGC12732, UGCA444, NGC2915, UGC07603 and IC2574. Model fit for each galaxy is denoted by solid blue line. Blue dashed line denotes the fit for M31. Lines are shifted along r for clarity.

5. Tully–Fisher Relation

In order to calibrate the BTFR, we match from the reduced sample of 81 galaxies with the representative sample of 118 galaxies studied by Lelli et al. [19]. After removing two outliers UGC00128 and UGCA444, we identify 56 matching and 13 additional objects from the SPARC database [19]. The final sample accounts for 69 galaxies for fitting the observational BTFR. For consistency, we account for the errors on the mass due to the uncertainty of the measured distances. We used the following expression:

$$\log \mathcal{M}_b = \alpha \log V_{flat} + \beta, \tag{8}$$

where α is the power index (slope) and β (intercept) is the multiplication factor i.e., $A = 10^{\beta}$ and V_{flat} is the velocity estimated for the flat part of the curve. The RC profiles have a rather complex shape, so that there are several velocities that could be identified, such as peak velocity (maximum observed velocity at smaller radii), flat velocity (at most of the radii where velocity does not change significantly, remaining almost constant) and terminal velocity (at the very outer part of the disk). In order to minimize ambiguity, we use the values for V_{flat} reported by Lelli et al. [19]. The relation between V_g and V_{flat} is shown in Figure 3 (top panel). V_{flat} is similar to V_g predicted by our model, but even a small difference between these values leads to changes in α and β. Also, it is important to note that using data for mass and velocity estimation by Lelli et al. [19] in Equation (8) leads to certain values α and β, while our model accounts for fitted values for V_{flat} and ρ_0 using Equation (3). ρ_0 is used to estimate baryonic mass for each galaxy in the sample (for details, see Appendix C) which are implemented in Equation (8). Obtained values of parameters α and β are a direct consequence of velocity and mass estimation. Therefore, for BTFR, we obtain the following:

$$\log \mathcal{M}_b = (3.7 \pm 0.2) \log V_{flat} + (2.7 \pm 0.4). \tag{9}$$

The results of our estimates are shown in Figure 3 (middle panel). The slope is in agreement with values inferred from the literature, e.g., kinematic survey of spiral and irregular galaxies [33], predictions by MOND [6]. For the reference value of the BTFR intercept, we adopt $\beta = (2.27 \pm 0.19)$ [19]. Our estimation of β differs by $\sim$0.4, which is just partly due to an overestimation of the total mass; adoption of constant SMD would lead to the mass estimation change by a factor of $\sim$0.3 at most compared to averaged exponential distribution Appendix C. However, fitting the RC by an expression given in Equation (3) implies that the BTFR is shifted upwards (Figure 3 middle and bottom panels). Such a consistent systematic offset for β is a clear indicator of under-fitting (high bias), which is no surprise given the simplicity of the current model that relies only on the observed kinematics. More accurate estimates of the β are possible by increasing the complexity of the model, combined with the additional information from the observed luminosity profiles and the inclusion of the gas component. Such a scenario would allow one to apply the soliton theory through the framework developed by Lelli et al. [19].

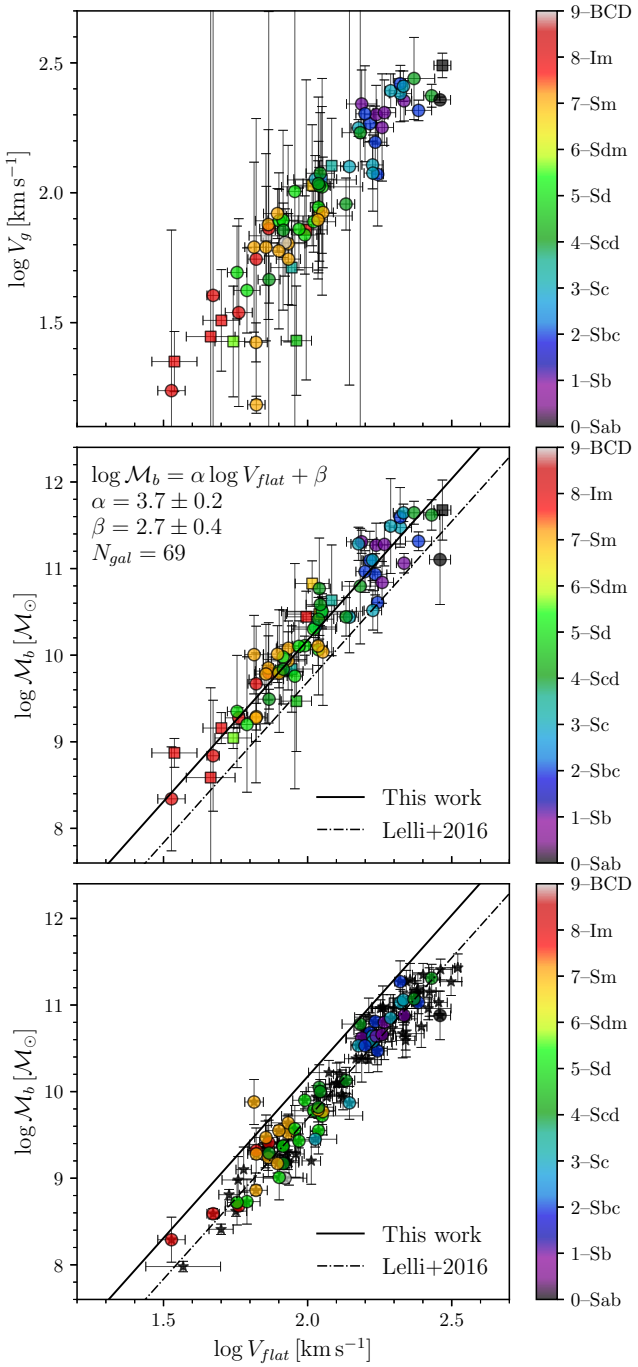

Figure 3. Relation $V_g - V_{flat}$ (upper panel). BTFR relation for our model for the sample of 69 galaxies, middle panel. Here, circles denote 56 objects matched with the original sample by Lelli et al. [19]. Squares denote an additional 13 found in SPARC. Bottom panel: canonical BTFR reported by Lelli et al. [20] for 116 spirals in SPARC. Discarded objects are denoted by filled stars. A solid black line represents the best linear fit. Dashed-dotted line for $\alpha = 3.71$ and $\beta = 2.27$. Galaxies are color-coded by type.

6. Discussion and Conclusions

Our model is a direct analytical self-consistent solution of galaxy dynamics equations. The only assumption is the infinitely thin disk approximation and that the condition for the existence of a soliton is valid. As a result, there is a group velocity and particles trapped by the density wave will keep the constant group velocity V_g that only depends on the ratio of differential rotation with respect to SMD (even though both parameters could be

radius-dependent). Fitting the model (Equation (3)) allows us to directly estimate two fundamental galactic quantities: galactic angular rotation $\Omega = \sqrt{2}\kappa$ and SMD. With these quantities, we independently and accurately determine the total mass and angular velocity of the galaxy in a completely novel manner. The Tully–Fisher relation is obtained purely based on a dynamical model by [12,25] and without the assumption of additional mass components. This model provides a theoretical explanation of the empirical BTFRA (first panel of Figure 3).

The model with constant parameters is rather rigid when fitting the galaxy-rotation curves and it is not capable of fully describing the rotation curves for large galaxies for which the assumption of constant density over such a long scale is far from ideal, together with galaxies that show complex and peculiar features. This is one reason why wave group velocity V_g deviates up to a reasonable value to pure circular velocity V (there will always be some amount of stars and gas that have not yet been trapped by the wave). These extended profiles of differential rotation and equilibrium SMD will be a subject of a separate analysis by increasing the complexity of the model, i.e., assuming certain empirical dependence with distance (e.g., exponential or power-law profiles), including the gas component in the model, and consistently repeating the BTFR fitting experiment, completely within the framework proposed by Lelli et al. [19]. Moreover, such a model allows for probing soliton structures using numerical data from cosmological magnetohydrodynamical simulations of galaxy formations, specifically TNG50 (https://www.tng-project.org/, accessed on 20 July 2024) [34,35].

Probing the proposed nonlinear density wave theory by the empirically established baryonic Tully–Fisher relation gives the possibility to rely only on the observed RC from which the dynamical parameters are inferred without the need for models based on gas and stellar populations [13], for which the complexity is typically much higher than in our present case. Analyzing Figure 3 (middle panel), we can notice that estimated masses using our model are 2 or 3 times higher than reported in the research by Lelli et al. [19]. In our case, this is partly due to the simplicity of the model, we assumed no radial dependence for model parameters, relevant to the mass estimation; mainly, this is due to a novel theoretically derived expression for the rotation velocity used in the fitting procedure. That particular expression has been derived self-consistently, with no a priori assumed potential nor mass distribution, but it rather follows the exact solution of a nonlinear Schrödinger equation. It should result in more accurate mass estimation. Overestimation of the mass due to the model simplicity (constant SMD via parameter a) can be compensated by inclusion of gas; this has been neglected in this research. However, all models relying on RCs only typically suffer the same problem—large dependence on the model assumptions yielding masses that can differ by an order of magnitude. Our estimation, e.g., in the case of the M31 galaxy, is in good agreement with the result of kinematic research by Carignan et al. [31].

The gas component itself could also be treated in the same way. In that case, the dispersion relation contains an additional term regarding velocity dispersion but it will not change the shape of the rotational curve [12,21,25]; it can only slightly increase or decrease the intensity of the group velocity which is in favor of the present results. As far as the galactic period of rotation is concerned, further research is necessary and it will probably have some implication on the galactic evolution due to some preliminary N-body simulations [26]. There are two main steps in this research. The first one is the novel relationship for the rotational velocity derived self-consistently using a justified fluid description and the dynamics of the wave phenomena represents the observed pattern in the nonlinear regime very well. That velocity expression is rather general and the aim is to probe the generality on the larger sample of spiral galaxies by fitting the RC with no inclusion of any other but baryonic matter with only one free parameter; the remaining dependent parameters can be derived using the relation between SMD and epyciclic frequency via the group velocity of the wave. This is in contrast with the work in [12,26], where the velocity expression was validated by implementation of the SMD and angular velocity values estimated using observations independent of the RC. The second one is a

derivation of the Tully–Fisher relation using the exact rotation velocity and the estimated mass using the fitted result. Our initial assumptions do not involve any comparatively larger dark matter halo that supports the stability of the very thin galactic disk nor any modified gravity acting on galactic scales and yet yields to a self-consistent explanation of the baryonic Tully–Fisher relation with a slope close to 4 for rotating late-type spiral galaxies: $\mathcal{M}_b \propto V^{3.7}$. Regarding the alternative solutions based on modified gravity, our solution gives an additional advantage; contrary to the theory of modified gravity, this model has no assumption concerning mass distribution building the gravity potential nor gravity potential acting on that mass; even more, it can explain decreasing RC at the z-shift corresponding to the pick of galaxy formation with no dark matter at that stage. However, some recent gravitational lensing studies of galaxy clusters provide an indication for the existence of cluster-scale dark matter haloes, as well as for alternative dark matter scenarios, such as self-interacting dark matter (for a recent review on this topic, see, e.g., [36]). The mass-to-light ratio is beyond the scope of this research and it will be the subject of a separate paper involving the exact solution of the NLS equation for both stellar and gas components.

Author Contributions: Conceptualization, M.V. and P.J.; methodology, M.V.; software, D.S.; validation, D.S., M.V. and P.J.; formal analysis, D.S.; resources, D.S.; data curation, D.S.; writing—original draft preparation, M.V.; writing—review and editing, M.V. All authors have read and agreed to the published version of the manuscript.

Funding: Part of this research is supported by the Ministry of Education and Science of the Republic of Serbia (contract 451-03-9/2021-14/200002). M.V. and P. J. acknowledge the support by the Ministry of Science, Technological Development and Innovation of the Republic of Serbia (MSTDIRS) through contract no. 451-03-66/2024-03/200002 made with Astronomical Observatory (Belgrade) and Đ.S. acknowledges support from the Fonds de la Recherche Scientifique—FNRS (Belgium) under grants PDR T.0116.21 and №4.4503.19.

Data Availability Statement: Data are contained within the article.

Acknowledgments: *Software:* PYTHON [37], JUPYTER [38]; *Packages:* NUMPY and SCIPY [39], PANDAS [40]; *Data visualization:* MATPLOTLIB [41].

Conflicts of Interest: The authors declare no conflicts of interest.

Abbreviations

The following abbreviations are used in this manuscript:

Λ CDM	Lambda–Cold Dark Matter
MOND	Modified Newtonian Dynamics
NLS	Nonlinear Schrödinger
BTFR	Baryonic Tully–Fisher Relation
SPARC	Spitzer Photometry and Accurate Rotation Curves
SMD	Surface Mass Density
RC	Rotation Curve

Appendix A. Methods

We transform Equation (3) by substituting $\Omega = \sqrt{2}\kappa$ [42], and by eliminating the parameters a, b and c using a relation $a = b/c$. This transformation leads to four free parameters to be estimated from the fit, for which we use the notation $X = (x_0, x_1, x_2, x_3) \equiv (\kappa, \rho_0, \rho_a, T)$. The model equation is:

$$V(r;\kappa,\rho_0,\rho_a,T) = \sqrt{\frac{1}{2}\kappa^2 r^2 + \frac{2\pi G\rho_0\rho_a r}{\cosh\left(T\kappa\rho_a - \frac{\kappa^2\rho_a}{2\pi G\rho_0}r\right)}}V(r;X)$$
$$= \sqrt{\frac{1}{2}x_0^2 r^2 + \frac{Ax_1x_2r}{\cosh\left(x_0x_2x_3 - C\frac{x_0^2x_2}{x_1}r\right)}}, \tag{A1}$$

where $A = C^{-1} = 2\pi G$. We fit the model (Equation (A1)) to observations by minimizing the χ^2 loss [43]:

$$\chi^2 = \sum_i \left(\frac{O_i - C_i}{\sigma_i}\right)^2, \tag{A2}$$

where O_i and σ_i are observed data points and errors, respectively, and $C_i \equiv V(r_i;X)$ is the model prediction. Errors on the fit parameters are obtained by computing the covariances. We built an optimizer using PYTHON [37] for fitting the model to observations. Our model function (Equation (A1)) is highly nonlinear over all parameters and minimizing the loss is heavily influenced by the initial guess of the parameters during the fitting procedure. We therefore generate thousands of random initial starting conditions that are passed to the optimizer in order to ensure the fit will have converged to a global minimum.

Appendix B. Individual Fits

M31 was excluded from the sample analysis for consistency because it was not one of the provided galaxy types we used in the statistical analysis. The results for M31 are reported independently in Figure A1.

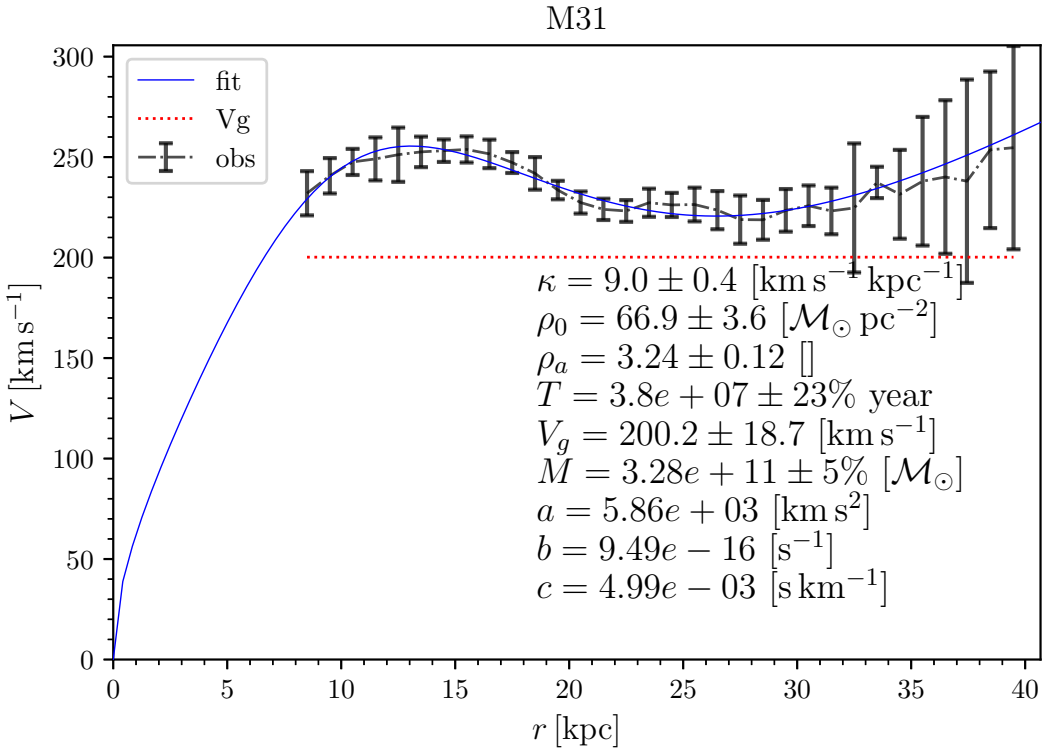

Figure A1. The best model fit for M31. Observational data points are denoted by a black dashed-dotted line. A red horizontal line denotes the group velocity V_g. A solid blue line represents the best fit. Relevant quantities are listed for guidance.

The results of the individual fits to the initial sample of 115 galaxies are listed below (Figures A2–A16). The notation is the same as in Figure A1.

Appendix C. Mass

Using SMD as a constant averaged value obtained by fitting the parameters a, b and c from Equation (3) leads to a different mass value compared to the value that would be obtained if SMD were an exponential function of the radius of the galactic disk. We show that in the case of the M31 galaxy, these two values differ by less than few percent. Let us assume SMD to be an exponential function of the radius following the results obtained by [44], Figure 2b. The estimated mass is

$$M_{exp} = 2\pi\Sigma_0 R_d^2[1 - e^{-R/R_d}(1 + \frac{R}{R_d})], \tag{A3}$$

where Σ_0 is the value of the SMD at a certain radius, in the particular case of M31 it is at 1 kpc, being $10^3 M_\odot / pc^2$ and $R_d = 10$ kpc following the exponential drop of M31 SMD given in Figure 2 of [44]. Averaging the SMD over the total radius, the mass expression would read as:

$$M_c = 2\pi\Sigma_0 R_d R[1 - e^{-R/R_d}], \tag{A4}$$

where we used the averaged function $\overline{\rho} = \frac{1}{R}\int_0^R \Sigma_0 e^{-r/R_d} dr$. In both Equations (A3) and (A4), the expressions in capital brackets tends to 1 for $R > R_d$, and consequently $M_{exp} < M_c$. In the latter case, for the total radius of $R = 30$ kpc the mass is approximately $2.5 \times 10^{11} M_\odot$. On the other hand, using the formula for mass estimation in this research $M_b = 2\pi\rho_0 R^2$, where ρ_0 is the equilibrium SMD that also must be radius-dependent, but in the fitting procedure it has an averaged value of $\sim 70 M_\odot / pc^2$; we obtain the mass to be $3.3 \times 10^{11} M_\odot$. The ratio $\frac{M_b}{M_c}$ strongly depends on the exact value of Σ_0, R_d and of the total radius R. However, the averaging SMD is partly responsible for the almost double mass estimation and consequently it interferes with the value of the intercept in the BTFR. Note that we have not compared our result with the original exponential mass M_{exp} since the averaged SMD value ρ_0 in our research does not correspond with Σ_0 but rather $\Sigma_0 R_d$ is to be compared with $\rho_0 R$.

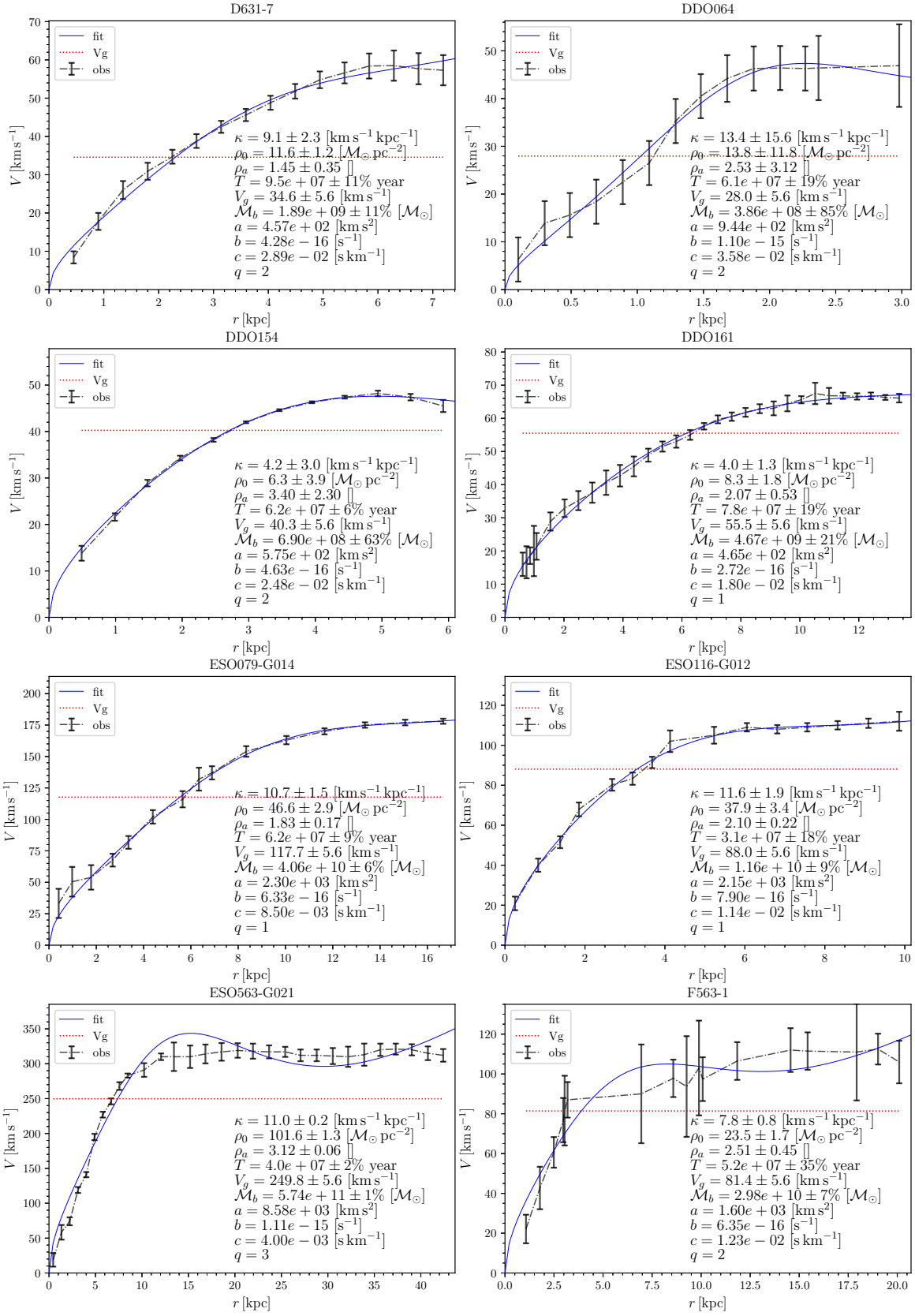

Figure A2. Model fits for D631-7, DDO064, DDO154, DDO161, ESO079-G014, ESO116-G012, ESO563-G021, F563-1.

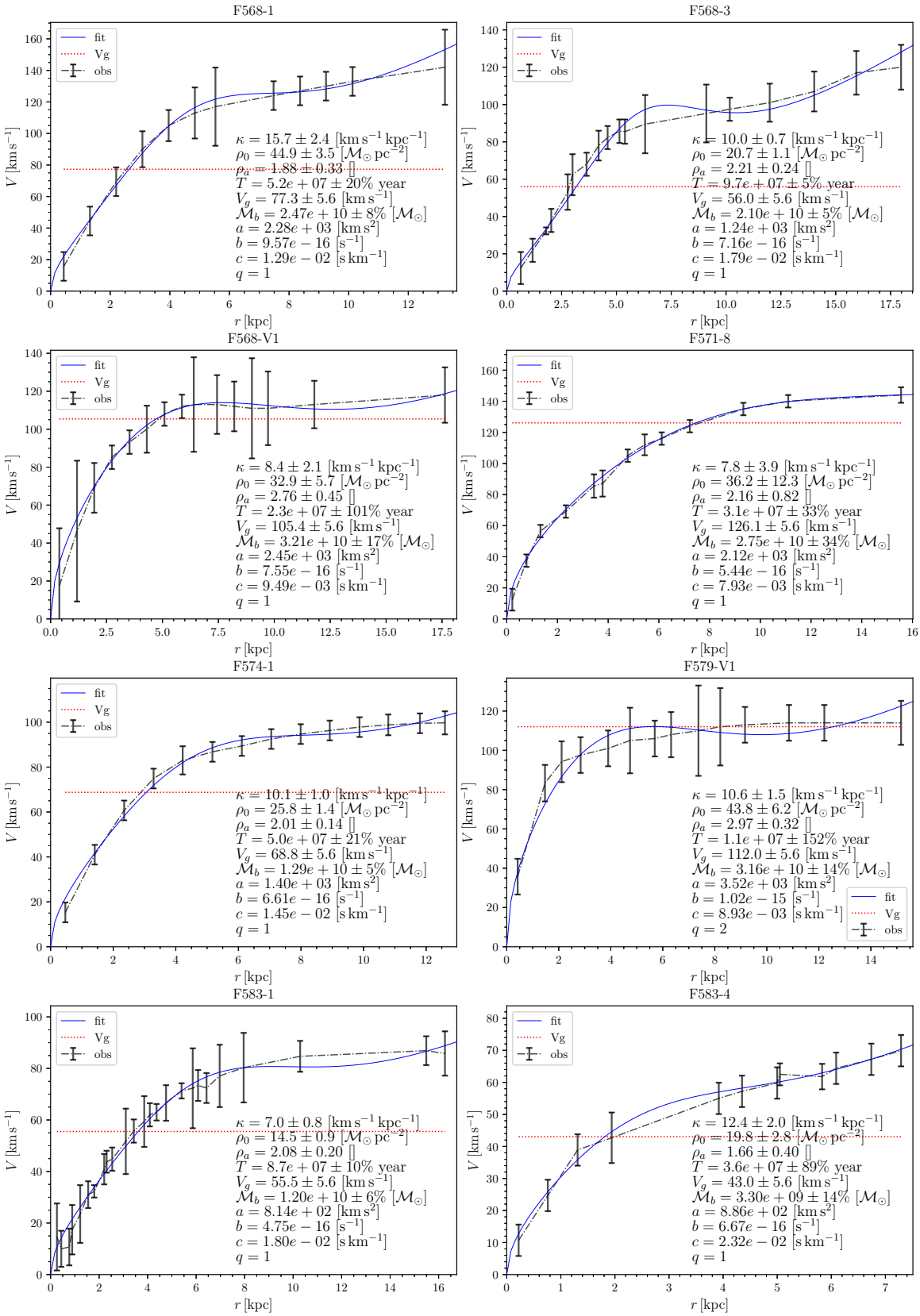

Figure A3. Model fits for F568-1, F568-3, F568-V1, F571-8, F574-1, F579-V1, F583-1, F583-4.

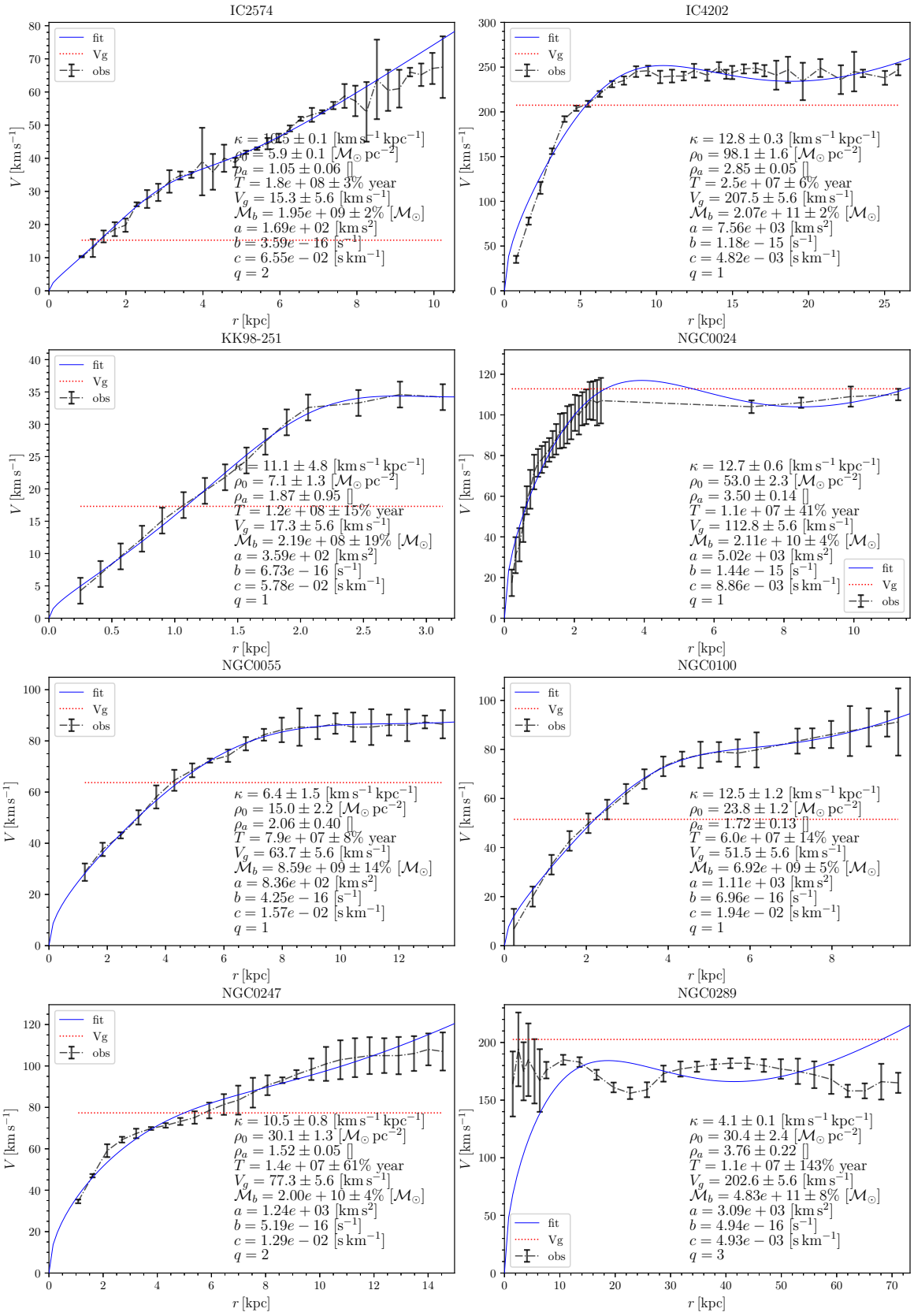

Figure A4. Model fits for IC2574, IC4202, KK98-251, NGC0024, NGC0055, NGC0100, NGC0247, NGC0289.

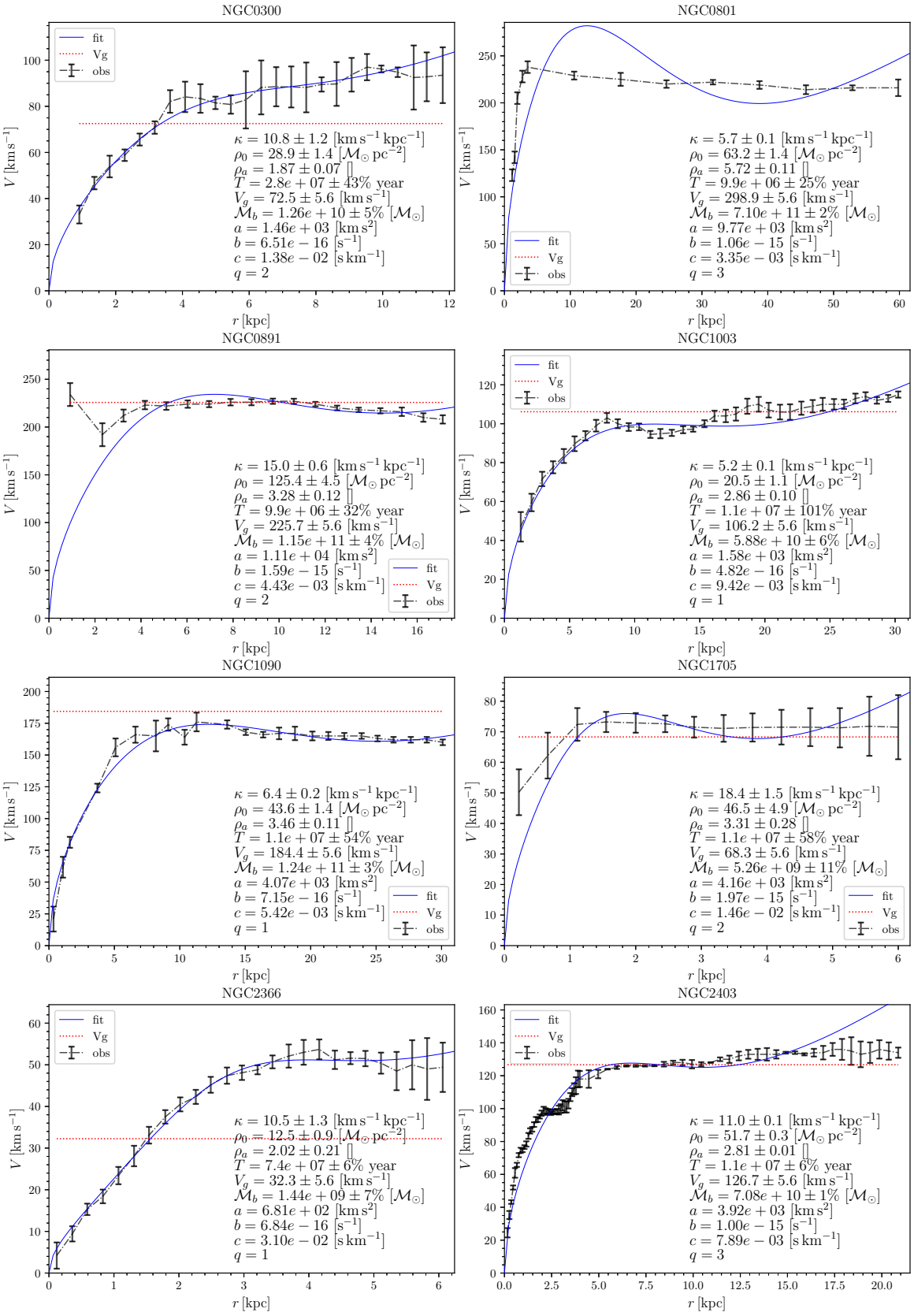

Figure A5. Model fits for NGC0300, NGC0801, NGC0891, NGC1003, NGC1090, NGC1705, NGC2366, NGC2403.

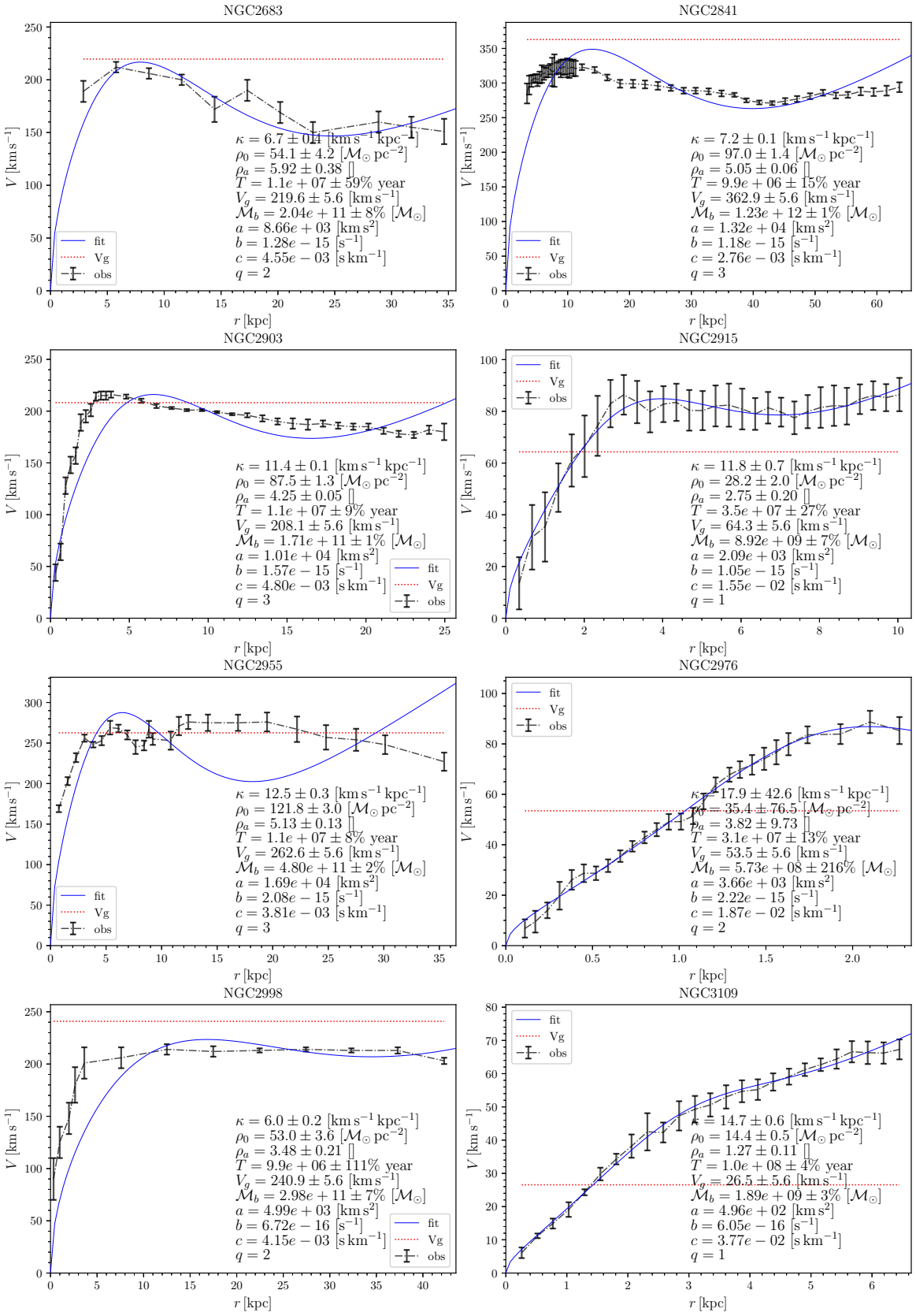

Figure A6. Model fits for NGC2683, NGC2841, NGC2903, NGC2915, NGC2955, NGC2976, NGC2998, NGC3109.

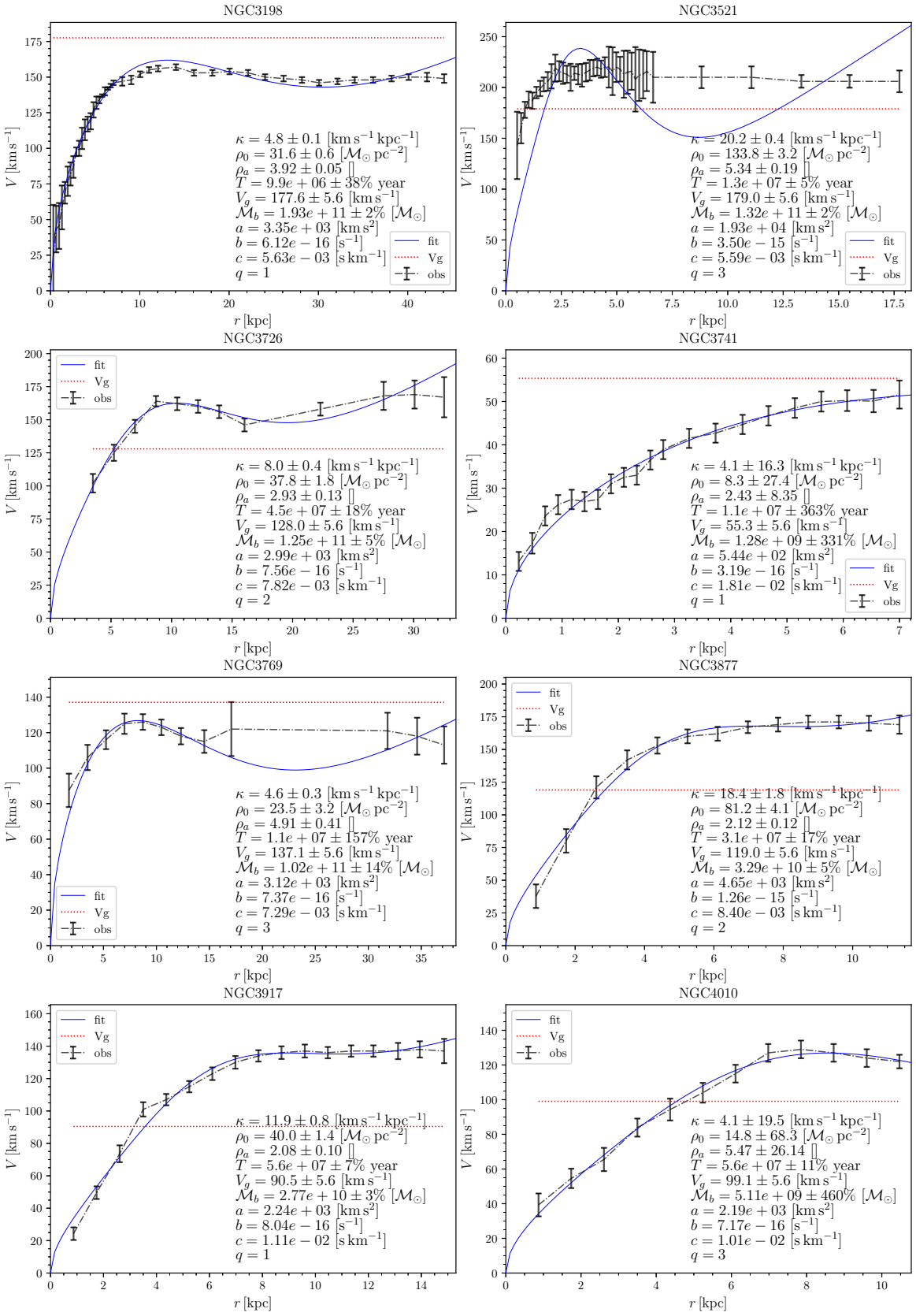

Figure A7. Model fits for NGC3198, NGC3521, NGC3726, NGC3741, NGC3769, NGC3877, NGC3917, NGC4010.

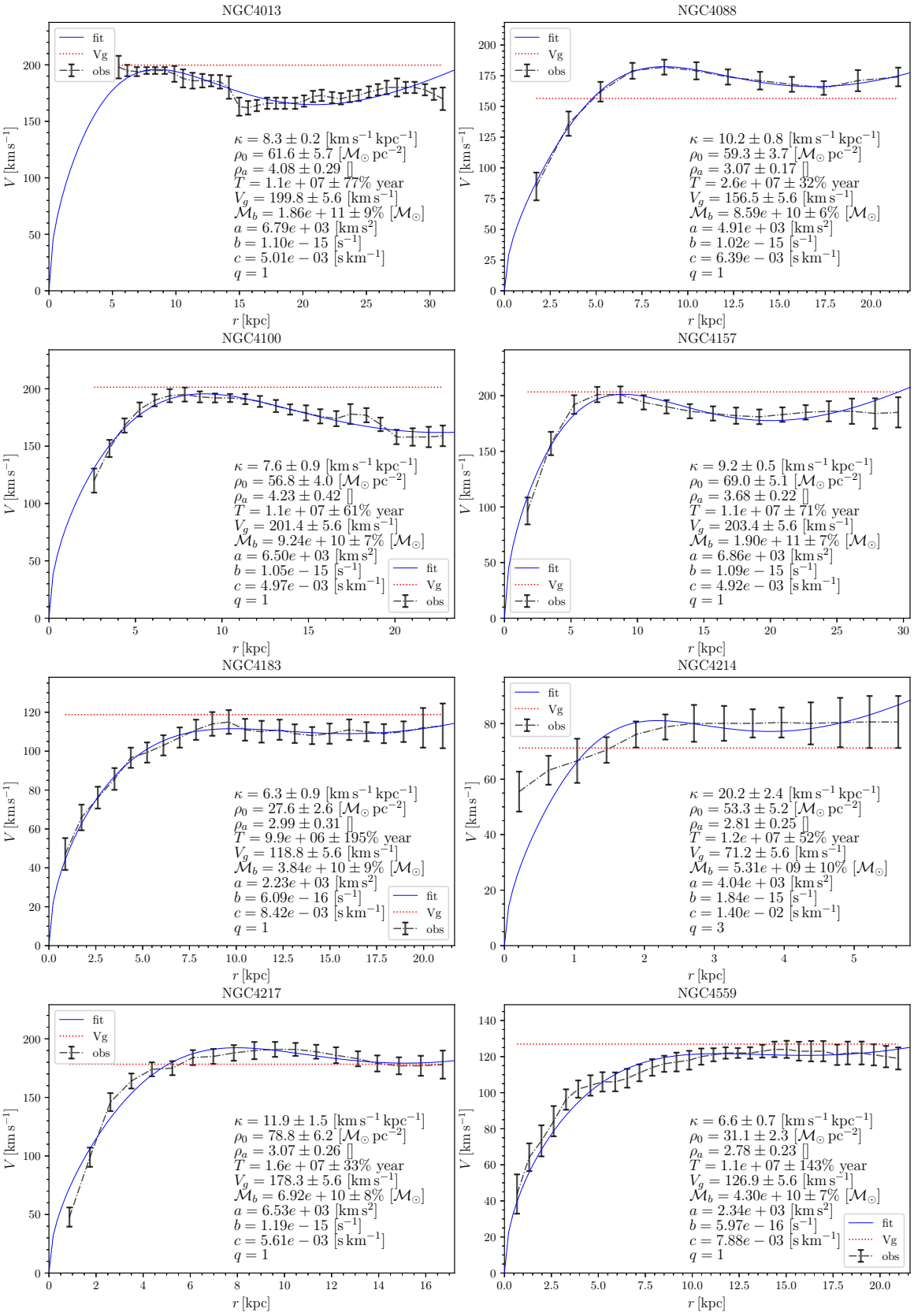

Figure A8. Model fits for NGC4013, NGC4088, NGC4100, NGC4157, NGC4183, NGC4214, NGC4217, NGC4559.

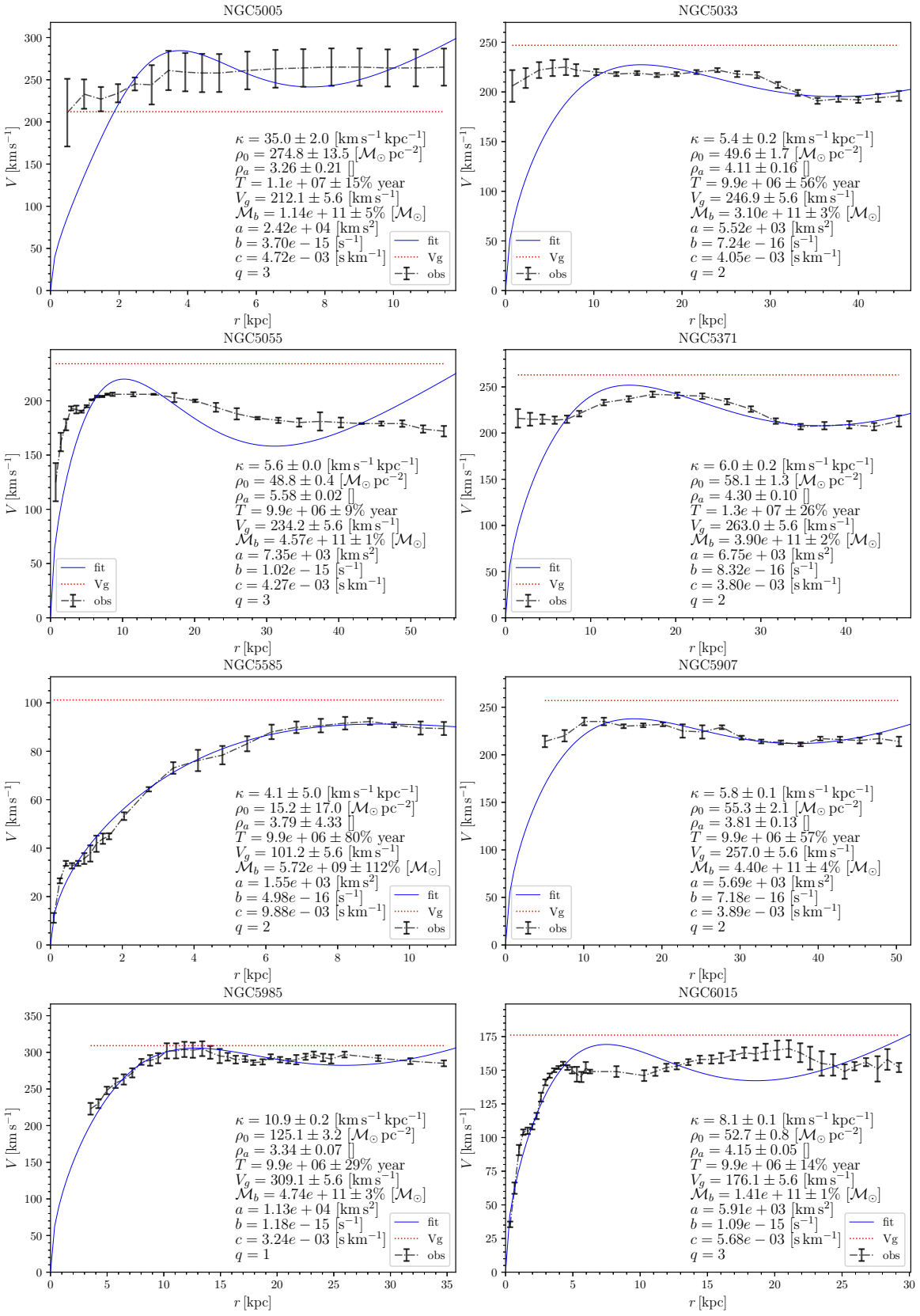

Figure A9. Model fits for NGC5005, NGC5033, NGC5055, NGC5371, NGC5585, NGC5907, NGC5985, NGC6015.

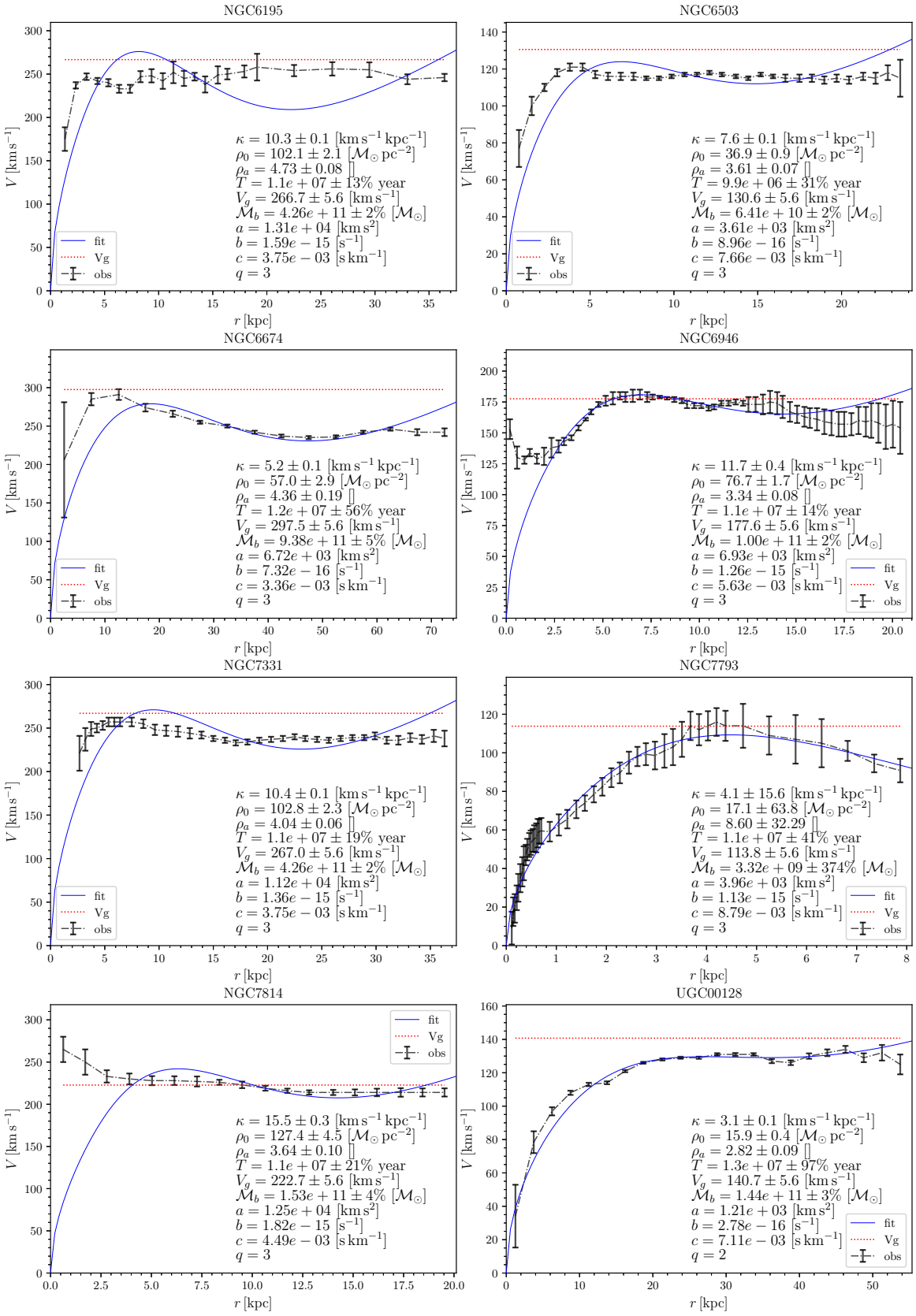

Figure A10. Model fits for NGC6195, NGC6503, NGC6674, NGC6946, NGC7331, NGC7793, NGC7814, UGC00128.

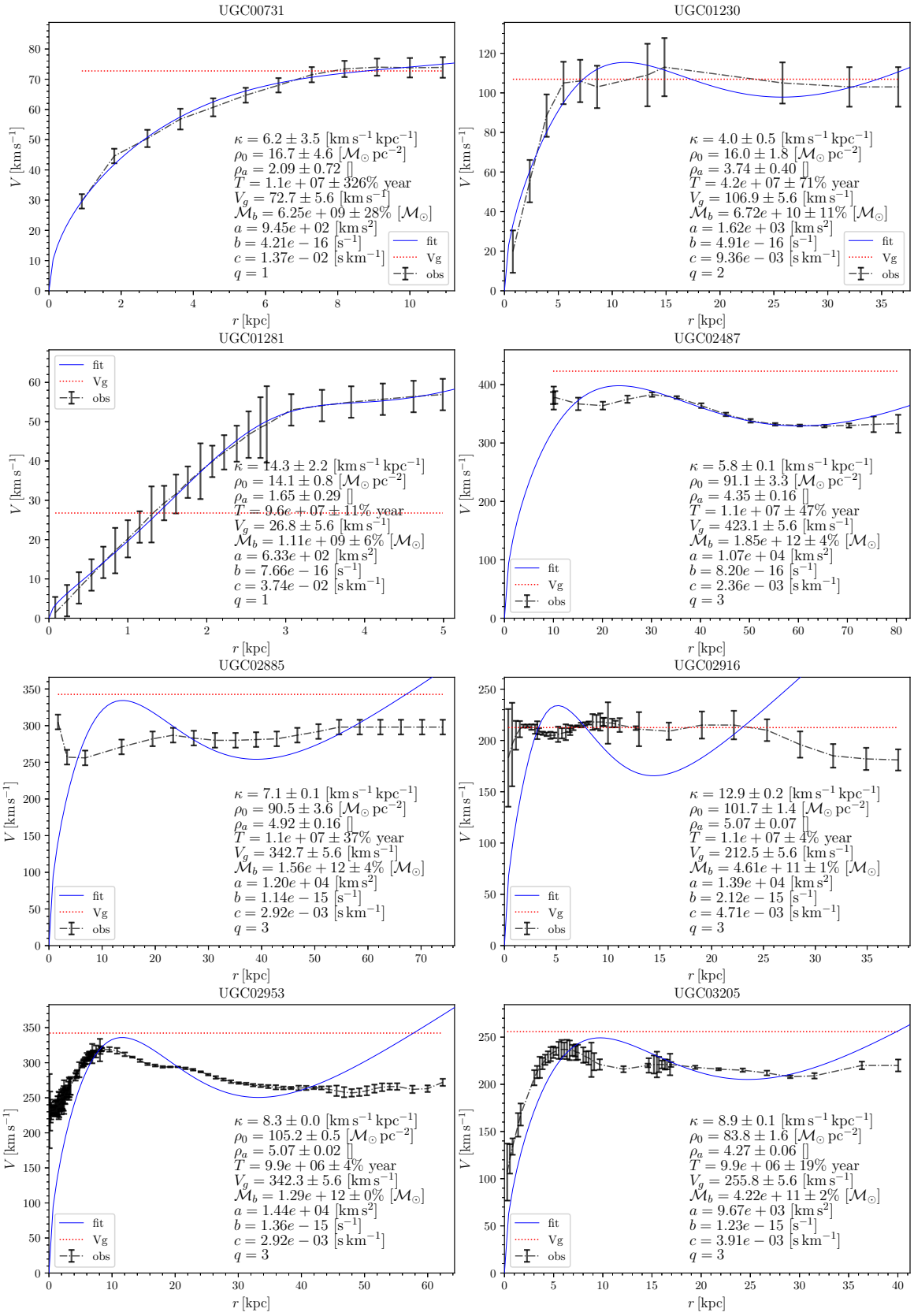

Figure A11. Model fits for UGC00731, UGC01230, UGC01281, UGC02487, UGC02885, UGC02916, UGC02953, UGC03205.

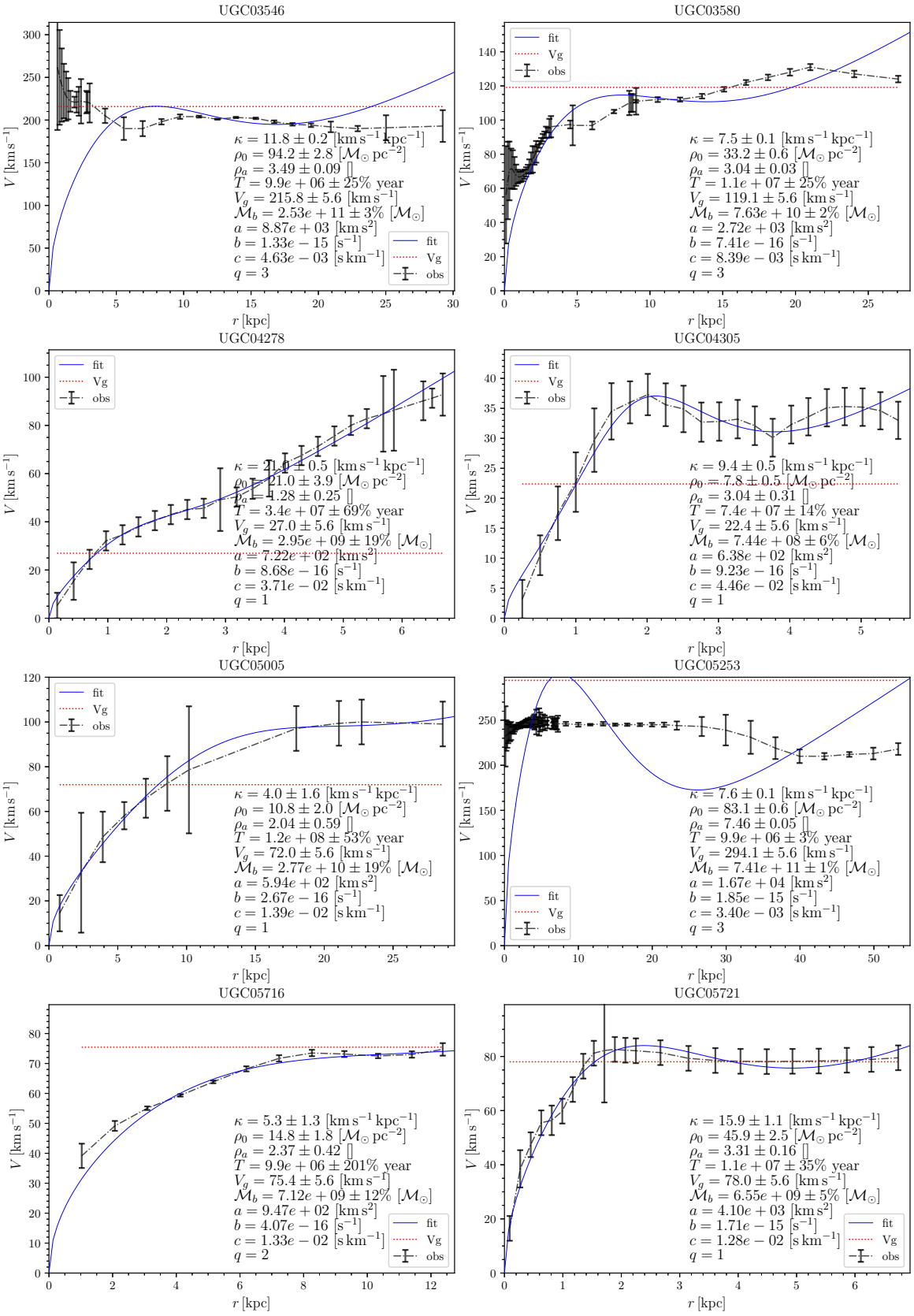

Figure A12. Model fits for UGC03546, UGC03580, UGC04278, UGC04305, UGC05005, UGC05253, UGC05716, UGC05721.

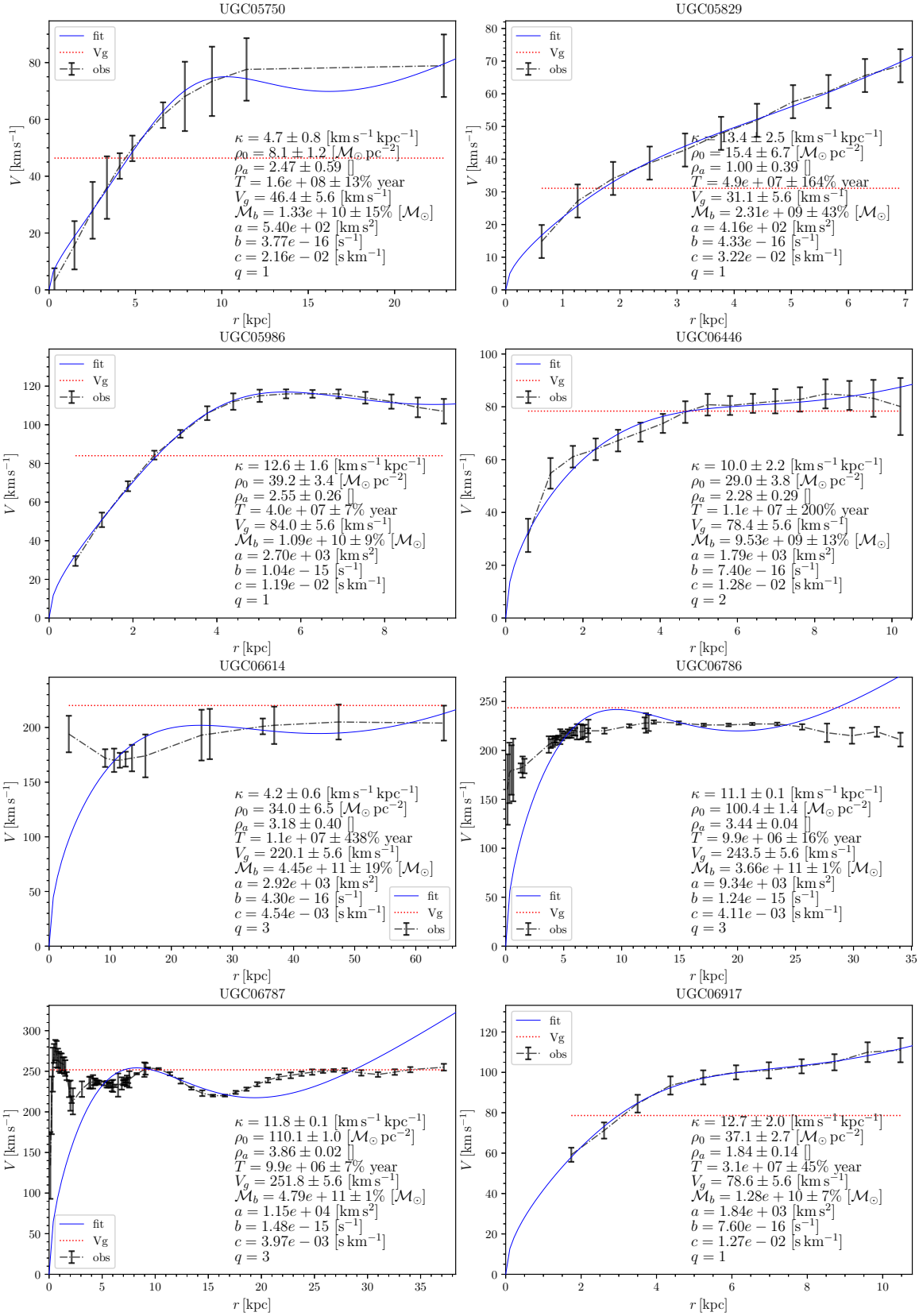

Figure A13. Model fits for UGC05750, UGC05829, UGC05986, UGC06446, UGC06614, UGC06786, UGC06787, UGC06917.

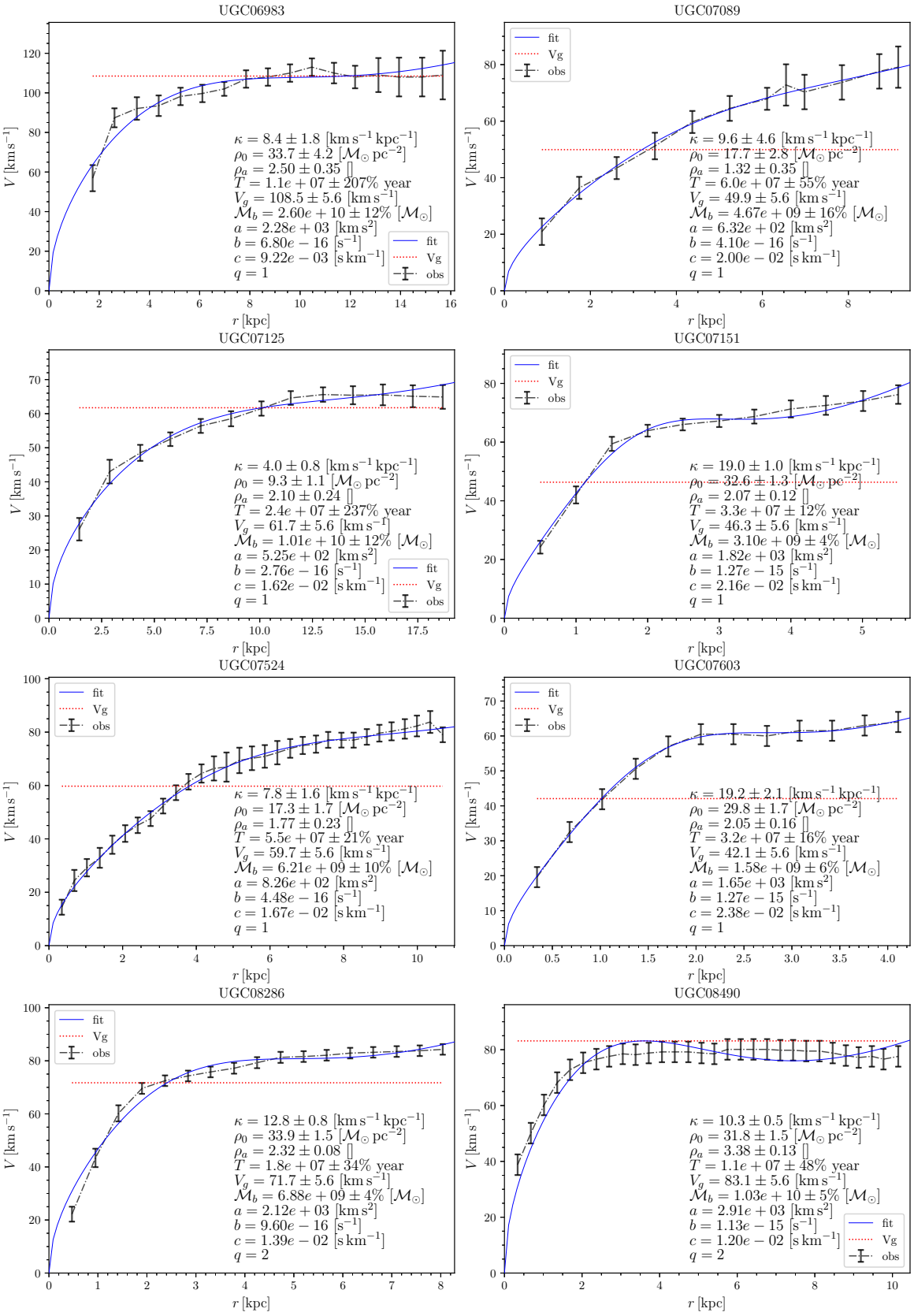

Figure A14. Model fits for UGC06983, UGC07089, UGC07125, UGC07151, UGC07524, UGC07603, UGC08286, UGC08490.

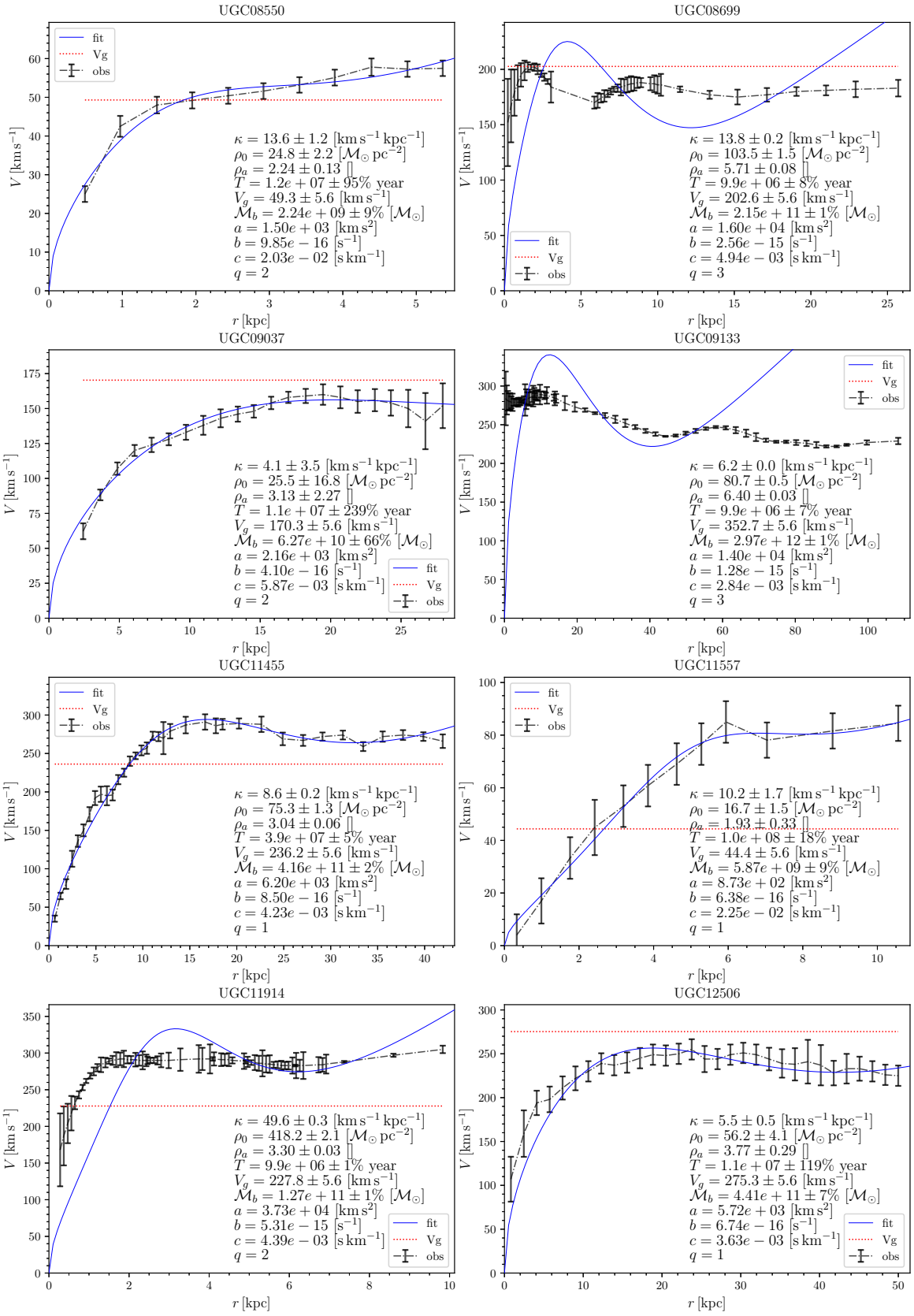

Figure A15. Model fits for UGC08550, UGC08699, UGC09037, UGC09133, UGC11455, UGC11557, UGC11914, UGC12506.

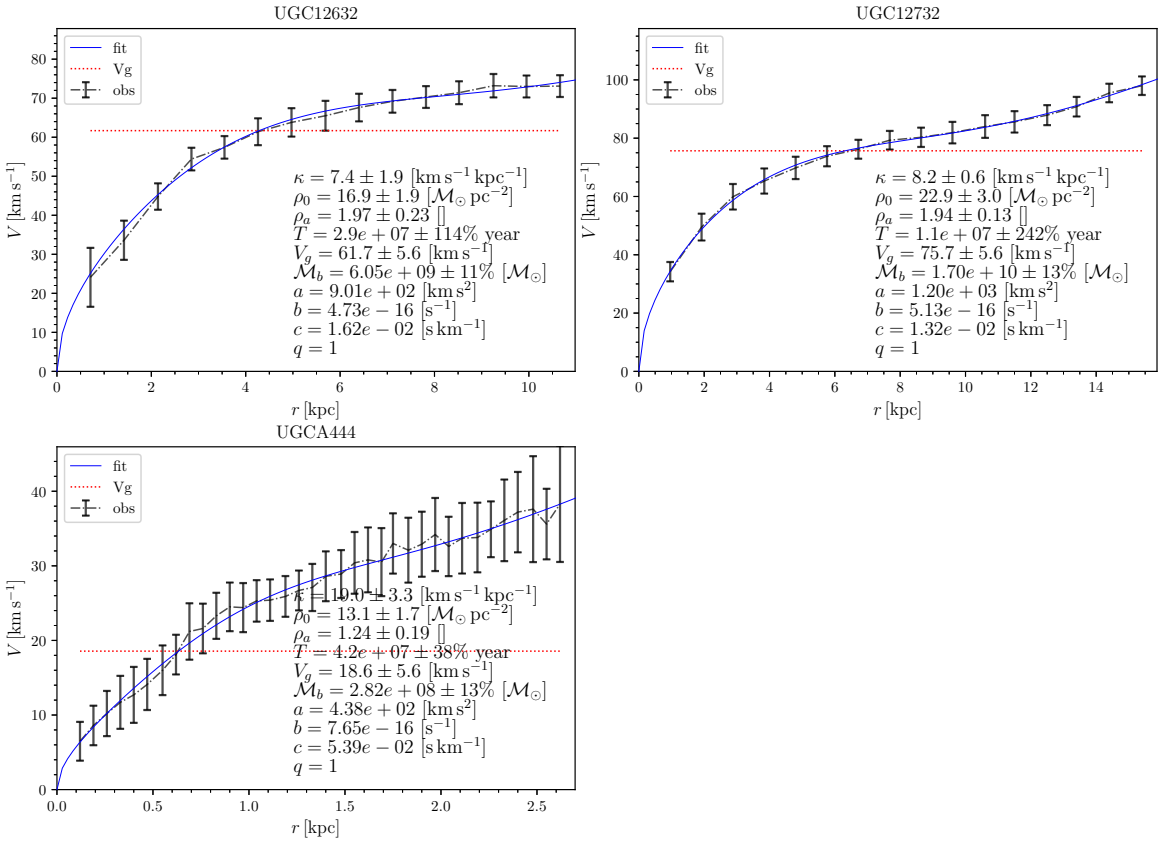

Figure A16. Model fits for UGC12632, UGC12732, UGCA444.

References

1. Tully, R.B.; Fisher, J.R. A New Method of Determining Distances to Galaxies. *Astron. Astrophys.* **1977**, *54*, 661.
2. Sakai, S.; Mould, J.R.; Hughes, S.M.; Huchra, J.P.; Macri, L.M.; Kennicutt, R.C., Jr.; Gibson, B.K.; Ferrarese, L.; Freedman, W.L.; Han, M.; et al. The Hubble Space Telescope Key Project on the Extragalactic Distance Scale. XXIV. The Calibration of Tully–Fisher Relations and the Value of the Hubble Constant. *Astrophys. J.* **2000**, *529*, 698. [CrossRef]
3. Trujillo-Gomez, S.; Klypin, A.; Primack, J.; Romanowsky, A.J. Galaxies in λCDM with Halo Abundance Matching: Luminosity-Velocity Relation, Baryonic Mass-Velocity Relation, Velocity Function, and Clustering. *Astrophys. J.* **2011**, *742*, 16. [CrossRef]
4. De Rossi, M.E.; Tissera, P.B.; Pedrosa, S.E. Impact of supernova feedback on the Tully–Fisher relation. *Astron. Astrophys.* **2010**, *519*, A89. [CrossRef]
5. Tonini, C.; Maraston, C.; Thomas, D.; Devriendt, J.; Silk, J. Hierarchical models of high-redshift galaxies with thermally pulsing asymptotic giant branch stars: Comparison with observations. *Mon. Not. R. Astron. Soc.* **2010**, *403*, 1749. [CrossRef]
6. Milgorm, M. A modification of the Newtonian dynamics as a possible alternative to the hidden mass hypothesis. *Astrophys. J.***1983**, *270*, 371. [CrossRef]
7. Sanders, R.H. Anty-gravity and galaxy rotation curves. *Astron. Astrophys.* **1984**, *136*, L21.
8. Moffat, J.W. Scalar–tensor–vector gravity theory. *J. Cosmol. Astropart. Phys.* **2006**, *03*, 004. [CrossRef]
9. Freeman, K.C. On the disks of spiral and S0 galaxies. *Astrophys. J.* **1970**, *170*, 3.
10. Verheijen, M.A. The Ursa Major Cluster of Galaxies; Tully–Fisher Relations and Dark Matter. *Astrophys. J.* **2001**, *563*, 694. [CrossRef]
11. Bell, E.F.; de Jong, R.S. Stellar Mass-to-Light Ratios and the Tully–Fisher Relation. *Astrophys. J.* **2001**, *550*, 212. [CrossRef]
12. Vukcevic, M. The Spiral galaxies flat rotational velocity curve explained by the constant group velocity of a nonlinear density wave. *Astrophys. J.* **2021**, *161*, 118. [CrossRef]
13. McGaugh, S.S. The Baryonic Tully–Fisher Relation of Gas-Rich Galaxies as a Test of λCdm and Mond. *Astrophys. J.* **2012**, *143*, 40. [CrossRef]
14. Gurovich, S.; Freeman, K.; Jerjen, H.; Staveley-Smith, L.; Puerari, I. The slope of the baryonic tully–fisher relation. *Astrophys. J.* **2010**, *140*, 663. [CrossRef]
15. Trachternach, C.; De Blok, W.J.G.; McGaugh, S.S.; Van der Hulst, J.M.; Dettmar, R.J. The baryonic Tully–Fisher relation and its implication for dark matter halos. *Astron. Astrophys.* **2010**, *505*, 577. [CrossRef]
16. Stark, D.V.; McGaugh, S.S.; Swaters, R.A. A first attempt to calibrate the baryonic Tully–Fisher relation with gas-dominated galaxies. *Astrophys. J.* **2009**, *138*, 392. [CrossRef]

17. Pfenniger, D.; Revaz, Y. The Baryonic Tully–Fisher relation revisited. *Astron. Astrophys.* **2005**, *431*, 511. [CrossRef]
18. McGaugh, S.S.; Schombert, J.M.; Bothun, G.D.; De Blok, W.J.G. The Baryonic Tully–Fisher Relation. *Astrophys. J.* **2000**, *533*, L99. [CrossRef] [PubMed]
19. Lelli, F.; McGaugh, S.S.; Schombert, J.M. The small scatter of the baryonic Tully–Fisher relation. *Astrophys. J.* **2016**, *816*, L14. [CrossRef]
20. Lelli, F.; McGaugh, S.S.; Schombert, J.M. SPARC: Mass models for 157 disk galaxies with SPITZER photometry and accurate rotation curves. *Astrophys. J.* **2016**, *152*, 157. [CrossRef]
21. Vukcevic, M. Nonlinear Density Wave Theory in a Gaseous Disk. *Astrophys. J.* **2024**, *167*, 15. [CrossRef]
22. Henrikseni, R.N. Transient Spiral Arms in Isothermal Stellar Systems. *arXiv* **2012**, arXiv:1207.5430.
23. Lin, C.C.; Shu, F.H. On the Spiral Structure of Disk Galaxies. *Astrophys. J.* **1964**, *140*, 646. [CrossRef]
24. Shu, F.H. Six decades of spiral density wave theory. *Annu. Rev. Astron. Astrophys.* **2016**, *54*, 667. [CrossRef]
25. Vukcevic, M. Non-linear density wave solutions for different models of galaxies. *Mon. Not. R. Astron. Soc.* **2014**, *441*, 565. [CrossRef]
26. Vukcevic, M.; Zekovic, V.; Radeta, M. Spiral structure of the galactic disk and its influence on the rotational velocity curve. *Astron. Nachrichten* **2022**, *343*, e210108. [CrossRef]
27. Corbelli, E.; Lorenzoni, S.; Walterbos, R.; Braun, R.; Thilker, D. A wide-field H I mosaic of Messier 31 II. The disk warp, rotation, and the dark matter halo. *Astron. Astrophys.* **2010**, *511*, A89. [CrossRef]
28. McGaugh, S.S.; Lelli, F.; Schombert, J.M. Radial Acceleration Relation in Rotationally Supported Galaxies. *Phys. Rev. Lett.* **2016**, *117*, 201101. [CrossRef]
29. Evans, N.W.; Wilkinson, M.I. The mass of the Andromeda galaxy. *Mon. Not. R. Astron. Soc.* **2000**, *316*, 929. [CrossRef]
30. Hartwick, F.D.A.; Sargent, W.L.W. The mass of M31 as determined from the motions of its globular clusters. *Astrophys. J.* **1974**, *190*, 283.
31. Carignan, C.; Chemin, L.; Huchtmeier, W.K.; Lockman, F.J. The extended H I rotation curve and mass distribution of M31. *Astrophys. J.* **2006**, *641*, L109. [CrossRef]
32. Chemin, L.; Carignan, C.; Foster, T. HI kinematics and dynamics of Messier 31. *Astrophys. J.* **2009**, *705*, 1395. [CrossRef]
33. Torres-Flores, S.; Epinat, B.; Amram, P.; Plana, H.; de Oliveira, C.M. GHASP: An Hαkinematic survey of spiral and irregular galaxies–IX. The near-infrared, stellar and baryonic Tully–Fisher relations. *Mon. Not. R. Astron. Soc.* **2011**, *416*, 1936. [CrossRef]
34. Nelson, D.; Pillepich, A.; Springel, V.; Pakmor, R.; Weinberger, R.; Genel, S.; Torrey, P.; Vogelsberger, M.; Marinacci, F.; Hernquist, L. First results from the TNG50 simulation: Galactic outflows driven by supernovae and black hole feedback. *Mon. Not. R. Astron. Soc.* **2019**, *490*, 3234. [CrossRef]
35. Pillepich, A.; Nelson, D.; Springel, V.; Pakmor, R.; Torrey, P.; Weinberger, R.; Vogelsberger, M.; Marinacci, F.; Genel, S.; van der Wel, A.; et al. First results from the TNG50 simulation: The evolution of stellar and gaseous discs across cosmic time. *Mon. Not. R. Astron. Soc.* **2019**, *490*, 3196. [CrossRef]
36. Natarajan, P.; Williams, L.L.R.; Bradač, M.; Grillo, C.; Ghosh, A.; Sharon, K.; Wagner, J. Strong Lensing by Galaxy Clusters. *arXiv* **2010**, arXiv:2403.06245. [CrossRef]
37. Van Rossum, G.; Drake, F.L., Jr. *Python Reference Manual*; Centrum voor Wiskunde en Informatica Amsterdam: Amsterdam, The Netherlands, 1995.
38. Thomas, K.; Benjamin, R.K.; Fern, o.P.; Brian, G.; Matthias, B.; Jonathan, F. *Positioning and Power in Academic Publishing: Players, Agents and Agendas*, 2016th ed.; Loizides, F., Scmidt, B., Eds.; IOS Press: Amsterdam, The Netherlands, 2016; pp. 87–90.
39. Van Der Walt, S.; Colbert, S.C.; Varoquaux, G. The NumPy Array: A Structure for Efficient Numerical Computation. *Comput. Sci. Eng.* **2011**, *13*, 22. [CrossRef]
40. McKinney, W. Data Structures for Statistical Computing in Python. In Proceedings of the 9th 297 Python in Science Conference, Austin, TX, USA, 28–30 June 2010; Volume 445, pp. 51–56.
41. Hunter, J.D. Matplotlib: A 2D graphics environment. *Comput. Sci. Eng.* **2007**, *9*, 90. [CrossRef]
42. Binney, J.; Tremaine, S. *Galactic Dynamics*, 2nd ed.; Princeton University Press: Princeton, NJ, USA, 2008.
43. Andrae, R.; Schulze-Hartung, T.; Melchior, P. Dos and don'ts of reduced chi-squared. *arXiv* **2010**, arXiv:1012.3754.
44. Sofue, Y. Radial distributions of surface mass density and mass-to-luminosity ratio in spiral galaxies. *Publ. Astron. Soc. Jpn.* **2018**, *70*, 31. [CrossRef]